

Theory of Dyakonov–Tamm waves at the planar interface of a sculptured nematic thin film and an isotropic dielectric material

Kartiek Agarwal,^{1,2} John A. Polo, Jr.,³ and Akhlesh Lakhtakia^{2,4}‡

¹ Department of Electrical Engineering, Indian Institute of Technology Kanpur, Kanpur 208016, India

² NanoMM—Nanoengineered Metamaterials Group, Department of Engineering Science and Mechanics, Pennsylvania State University, University Park, PA 16802, USA

³ Department of Physics and Technology, Edinboro University of Pennsylvania, Edinboro, PA 16444, USA

⁴ Department of Physics, Indian Institute of Technology Kanpur, Kanpur 208016, India

Abstract. In order to ascertain conditions for surface–wave propagation guided by the planar interface of an isotropic dielectric material and a sculptured nematic thin film (SNTF) with periodic nonhomogeneity, we formulated a boundary–value problem, obtained a dispersion equation therefrom, and numerically solved it. The surface waves obtained are Dyakonov–Tamm waves. The angular domain formed by the directions of propagation of the Dyakonov–Tamm waves can be very wide (even as wide as to allow propagation in every direction in the interface plane), because of the periodic nonhomogeneity of the SNTF. A search for Dyakonov–Tamm waves is, at the present time, the most promising route to take for experimental verification of surface–wave propagation guided by the interface of two dielectric materials, at least one of which is anisotropic. That would also assist in realizing the potential of such surface waves for optical sensing of various types of analytes infiltrating one or both of the two dielectric materials.

Keywords: Dyakonov wave, optical sensing, sculptured nematic thin film, surface wave, Tamm state, titanium oxide

‡ Corresponding author; e-mail:akhlesh@psu.edu

1. Introduction

In 1988, Dyakonov [1] theoretically predicted the propagation of electromagnetic waves guided by the planar interface of two homogeneous dielectric materials, one of which is isotropic and the other uniaxial with its optic axis aligned parallel to the interface. Since then, the existence of Dyakonov surface waves has been theoretically proved for many sets of dissimilar dielectric partnering materials, at least one of which is anisotropic [2, 3]. The possibility of the anisotropic partnering material being artificially engineered, either as a photonic crystal with a short period in comparison to the wavelength [4] or as a columnar thin film (CTF) [5], has also emerged. Just like that of many surface phenomena [6], the significance of Dyakonov surface waves for optical sensing applications is obvious: the disturbance of the constitutive properties of one or both of the two partnering materials—due to, say, infiltration by any analyte—could measurably change the characteristics of the chosen Dyakonov surface wave.

However, the directions of propagation of Dyakonov surface waves parallel to any suitable planar interface are confined to a very narrow angular domain, typically of the order of a degree or less [2, 7]. Not surprisingly, Dyakonov surface waves still remain to be experimentally observed. Clearly then, the potential of Dyakonov surface waves cannot be realized if they cannot be demonstrably excited; a wider angular domain is needed.

Recently, Lakhtakia and Polo [8] examined surface–wave propagation guided by the planar interface of an isotropic dielectric material and a chiral sculptured thin film [9] with its direction of periodic nonhomogeneity normal to the planar interface. The authors named the surfaces waves after Dyakonov and Tamm, the latter being the person who indicated the possibility of finding surface states of electrons at exposed planes of crystals and other periodic materials [10, 11]. The angular domain formed by the directions of propagation of the Dyakonov–Tamm waves turned out to be very wide, as much as 98° in one case for which realistic constitutive parameters of the two partnering materials were employed [8]. This implies that Dyakonov–Tamm waves could be detected much more easily than Dyakonov surface waves.

Chiral sculptured thin films (STFs) are structurally chiral materials:§ the

§ An object is said to be chiral if it cannot be made to coincide with its mirror-image by translations and/or rotations. There are two types of chiral materials: (i) microscopically or molecularly chiral materials, and (ii) structurally chiral materials. The first type of chiral materials either have chiral molecules or are composite materials made by embedding, e.g., electrically small helices in a host material. Materials comprising chiral molecules have been known for about two hundred years, as a perusal of an anthology of milestone papers [12] will show to the interested reader. These materials are generally (optically) isotropic [13]. Composite materials comprising electrically small [14, 15] chiral inclusions were first reported in 1898 [16], and these materials can be either isotropic [17, 18, 19] or anisotropic [20]. The first type of chiral materials can be considered as either homogeneous or nonhomogeneous continuums at sufficiently low frequencies. In contrast, the second type of chiral materials can only be nonhomogeneous and anisotropic continuums at the length–scales of interest, their constitutive parameters varying periodically in a chiral manner about a fixed axis. Take away the nonhomogeneity of a structurally chiral material, and its (macroscopic) chirality will also vanish

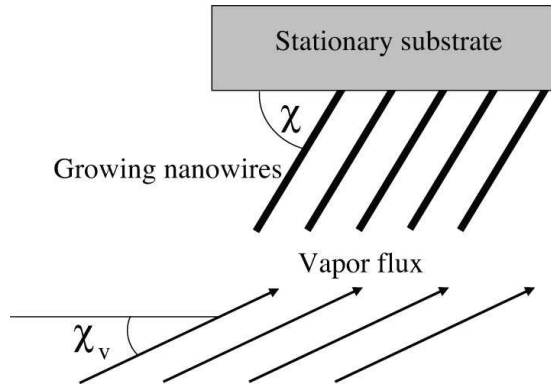


Figure 1. Schematic of a collimated vapor flux responsible for the growth of tilted straight nanowires growing at an angle $\chi \geq \chi_v$.

permittivity dyadic rotates at a uniform rate along the direction of nonhomogeneity. As a result, chiral STFs are periodically nonhomogeneous. Thus, in a chiral STF, structural chirality and periodic nonhomogeneity are inseparable. Is the huge angular existence domain of Dyakonov–Tamm waves for the case investigated by Lakhtakia and Polo [8] due to the periodicity or due to the structural chirality of the chiral STF? In order to answer this question, we devised a surface–wave–propagation problem wherein the chiral STF is replaced by a periodically nonhomogeneous and anisotropic material that is not structurally chiral. Specifically, we replaced the chiral STF with a sculptured nematic thin film (SNTF) [9].

CTFs, chiral STFs, and SNTFs are all fabricated by physical vapor deposition [9, 22, 23]. In the simplest implementation of this technique, a boat containing a certain material, say titanium oxide, is placed in an evacuated chamber. Under appropriate conditions, the material evaporates towards a substrate such that the vapor flux is highly collimated. The collimated vapor flux coalesces on the substrate as an ensemble of more or less identical and parallel nanowires, due to self–shadowing. If the substrate is held stationary during deposition, a CTF grows wherein the nanowires are straight and aligned at an angle $\chi \geq \chi_v$ with respect to the substrate plane, where χ_v is the angle between the collimated vapor flux and the substrate plane, as shown in Fig. 1. If the substrate is rotated about an axis passing normally through it, a chiral STF comprising helical nanowires grows. Finally, if the substrate is rocked about an axis tangential to the substrate plane, χ_v and χ are not constant and an SNTF grows. Scanning-electron-microscope images of a CTF, an SNTF, and a chiral STF are presented in Fig. 2.

This paper is organized as follows. Section 2 presents the boundary–value problem and the dispersion equation for the propagation of Dyakonov–Tamm waves guided by the interface of a homogenous, isotropic dielectric material and a periodically nonhomogeneous SNTF. Section 3 contains numerical results when the SNTF is chosen to be made of titanium oxide [5, 24]. An $\exp(-i\omega t)$ time–dependence is implicit, with ω [9, 21].

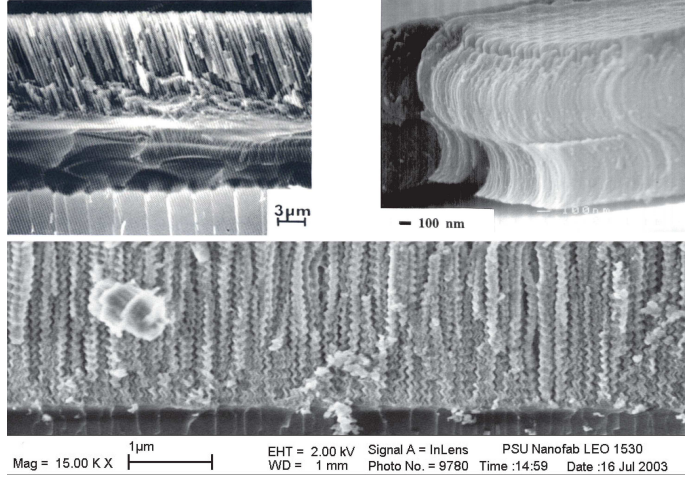


Figure 2. Scanning-electron-microscope images of sculptured thin films. Top left: columnar thin film; top right: sculptured nematic thin film; bottom: chiral sculptured thin film. Courtesy: Russell Messier and Mark Horn.

denoting the angular frequency. The free-space wavenumber, the free-space wavelength, and the intrinsic impedance of free space are denoted by $k_o = \omega \sqrt{\epsilon_o \mu_o}$, $\lambda_o = 2\pi/k_o$, and $\eta_o = \sqrt{\mu_o/\epsilon_o}$, respectively, with μ_o and ϵ_o being the permeability and permittivity of free space. Vectors are underlined, dyadics underlined twice; column vectors are underlined and enclosed within square brackets, while matrixes are underlined twice and similarly bracketed. Cartesian unit vectors are identified as \underline{u}_x , \underline{u}_y and \underline{u}_z . The dyadics employed in the following sections can be treated as 3×3 matrixes [25].

2. Formulation

2.1. Geometry and permittivity

Let the half-space $z \leq 0$ be occupied by an isotropic, homogeneous, nondissipative, dielectric material of refractive index n_s . The region $z \geq 0$ is occupied by an SNTF with a periodically nonhomogeneous permittivity dyadic given by [9]

$$\underline{\underline{\epsilon}}(z) = \epsilon_o \underline{\underline{S}}_z(\gamma) \cdot \underline{\underline{S}}_y(z) \cdot \underline{\underline{\epsilon}}_{ref}^o(z) \cdot \underline{\underline{S}}_y^T(z) \cdot \underline{\underline{S}}_z^T(\gamma), \quad z \geq 0. \quad (1)$$

The dyadic function

$$\begin{aligned} \underline{\underline{S}}_z(\gamma) = & (\underline{u}_x \underline{u}_x + \underline{u}_y \underline{u}_y) \cos \gamma \\ & + (\underline{u}_y \underline{u}_x - \underline{u}_x \underline{u}_y) \sin \gamma + \underline{u}_z \underline{u}_z \end{aligned} \quad (2)$$

contains γ as an angular offset, and the superscript T denotes the transpose. The dyadics

$$\underline{\underline{S}}_y(z) = (\underline{u}_x \underline{u}_x + \underline{u}_z \underline{u}_z) \cos [\chi(z)] + (\underline{u}_z \underline{u}_x - \underline{u}_x \underline{u}_z) \sin [\chi(z)] + \underline{u}_y \underline{u}_y \quad (3)$$

and

$$\underline{\underline{\epsilon}}_{ref}^o(z) = \epsilon_a(z) \underline{u}_z \underline{u}_z + \epsilon_b(z) \underline{u}_x \underline{u}_x + \epsilon_c(z) \underline{u}_y \underline{u}_y \quad (4)$$

depend on the vapor incidence angle

$$\chi_v(z) = \tilde{\chi}_v + \delta_v \sin\left(\frac{\pi z}{\Omega}\right) \quad (5)$$

that varies sinusoidally as a function of z with period 2Ω . Whereas $\tilde{\chi}_v \geq 0$, we have to ensure that $\chi_v(z) \in (0, \pi/2]$.

As no experimental data connecting $\epsilon_{a,b,c}(z)$ and $\chi(z)$ to $\chi_v(z)$ have been reported for SNTFs ($\delta_v \neq 0$), we decided to use available data for CTFs ($\delta_v = 0$). Optical characterization experiments on CTFs of titanium oxide at $\lambda_o = 633$ nm [24] lead to the following expressions for our present purpose:

$$\left. \begin{aligned} \epsilon_a(z) &= [1.0443 + 2.7394 v(z) - 1.3697 v^2(z)]^2 \\ \epsilon_b(z) &= [1.6765 + 1.5649 v(z) - 0.7825 v^2(z)]^2 \\ \epsilon_c(z) &= [1.3586 + 2.1109 v(z) - 1.0554 v^2(z)]^2 \\ \chi(z) &= \tan^{-1} [2.8818 \tan \chi_v(z)] \\ v(z) &= 2\chi_v(z)/\pi \end{aligned} \right\} . \quad (6)$$

Let us note that the foregoing expressions—with $v(z)$ independent of z —are applicable to CTFs produced by one particular experimental apparatus, but may have to be modified for CTFs produced by other researchers on different apparatuses.

Without loss of generality, we take the Dyakonov–Tamm wave to propagate parallel to the x axis in the plane $z = 0$. There is no dependence on the y coordinate, whereas the Dyakonov–Tamm wave must attenuate as $z \rightarrow \pm\infty$.

2.2. Field representations

In the region $z \leq 0$, the wave vector may be written as

$$\underline{k}_s = \kappa \underline{u}_x - \alpha_s \underline{u}_z, \quad (7)$$

where

$$\kappa^2 + \alpha_s^2 = k_o^2 n_s^2, \quad (8)$$

κ is positive and real-valued for unattenuated propagation along the x axis, and $\text{Im}[\alpha_s] > 0$ for attenuation as $z \rightarrow -\infty$. Accordingly, the field phasors in the region $z \leq 0$ may be written as [8]

$$\underline{E}(\underline{r}) = \left[A_s \underline{u}_y + A_p \left(\frac{\alpha_s}{k_o} \underline{u}_x + \frac{\kappa}{k_o} \underline{u}_z \right) \right] \exp(i \underline{k}_s \cdot \underline{r}), \quad z \leq 0, \quad (9)$$

and

$$\underline{H}(\underline{r}) = \eta_o^{-1} \left[A_s \left(\frac{\alpha_s}{k_o} \underline{u}_x + \frac{\kappa}{k_o} \underline{u}_z \right) - A_p n_s^2 \underline{u}_y \right] \exp(i \underline{k}_s \cdot \underline{r}), \quad z \leq 0, \quad (10)$$

where A_s and A_p are unknown scalars representing the amplitudes of s - and p -polarized components.

The field representation in the region $z \geq 0$ is more complicated. It is appropriate to write

$$\left. \begin{aligned} \underline{E}(\underline{r}) &= \underline{e}(z) \exp(i\kappa x) \\ \underline{H}(\underline{r}) &= \underline{h}(z) \exp(i\kappa x) \end{aligned} \right\}, \quad z \geq 0, \quad (11)$$

and create the column vector

$$[\underline{f}(z)] = [e_x(z) \quad e_y(z) \quad h_x(z) \quad h_y(z)]^T. \quad (12)$$

This column vector satisfies the matrix differential equation [9]

$$\frac{d}{dz} [\underline{f}(z)] = i [\underline{P}(z, \kappa)] \cdot [\underline{f}(z)], \quad z > 0, \quad (13)$$

where the 4×4 matrix

$$\begin{aligned} [\underline{P}(z, \kappa)] &= \\ &\omega \begin{bmatrix} 0 & 0 & 0 & \mu_o \\ 0 & 0 & -\mu_o & 0 \\ \epsilon_o [\epsilon_c(z) - \epsilon_d(z)] \cos \gamma \sin \gamma & -\epsilon_o [\epsilon_c(z) \cos^2 \gamma + \epsilon_d(z) \sin^2 \gamma] & 0 & 0 \\ \epsilon_o [\epsilon_c(z) \sin^2 \gamma + \epsilon_d(z) \cos^2 \gamma] & -\epsilon_o [\epsilon_c(z) - \epsilon_d(z)] \cos \gamma \sin \gamma & 0 & 0 \end{bmatrix} \\ &+ \kappa \frac{\epsilon_d(z) [\epsilon_a(z) - \epsilon_b(z)]}{\epsilon_a(z) \epsilon_b(z)} \sin \chi(z) \cos \chi(z) \begin{bmatrix} \cos \gamma & \sin \gamma & 0 & 0 \\ 0 & 0 & 0 & 0 \\ 0 & 0 & 0 & -\sin \gamma \\ 0 & 0 & 0 & \cos \gamma \end{bmatrix} \\ &+ \begin{bmatrix} 0 & 0 & 0 & -\frac{\kappa^2}{\omega \epsilon_o} \frac{\epsilon_d(z)}{\epsilon_a(z) \epsilon_b(z)} \\ 0 & 0 & 0 & 0 \\ 0 & \frac{\kappa^2}{\omega \mu_o} & 0 & 0 \\ 0 & 0 & 0 & 0 \end{bmatrix} \end{aligned} \quad (14)$$

and

$$\epsilon_d(z) = \frac{\epsilon_a(z) \epsilon_b(z)}{\epsilon_a(z) \cos^2 \chi(z) + \epsilon_b(z) \sin^2 \chi(z)}. \quad (15)$$

For $\sin \gamma = 0$, (13) splits into two autonomous matrix differential equations, each employing a 2×2 matrix [26].

Equation (13) has to be solved numerically. We used the piecewise uniform approximation technique [9] to determine the matrix $[\underline{N}]$ which appears in the relation

$$[\underline{f}(2\Omega)] = [\underline{N}] \cdot [\underline{f}(0+)] \quad (16)$$

to characterize the optical response of one period of the chosen SNTF. By virtue of the Floquet–Lyapunov theorem [27], we can define a matrix $[\underline{Q}]$ such that

$$[\underline{N}] = \exp \left\{ i2\Omega [\underline{Q}] \right\}. \quad (17)$$

Both $[\underline{N}]$ and $[\underline{Q}]$ share the same eigenvectors, and their eigenvalues are also related. Let $[\underline{t}]^{(n)}$, ($n = 1, 2, 3, 4$), be the eigenvector corresponding to the n th eigenvalue σ_n of $[\underline{N}]$; then, the corresponding eigenvalue α_n of $[\underline{Q}]$ is given by

$$\alpha_n = -i \frac{\ln \sigma_n}{2\Omega}. \quad (18)$$

2.3. Dispersion equation for Dyakonov–Tamm wave

For the Dyakonov–Tamm wave to propagate along the x axis, we must ensure that $\text{Im}[\alpha_{1,2}] > 0$, and set

$$[\underline{f}(0+)] = \begin{bmatrix} [\underline{t}]^{(1)} & [\underline{t}]^{(2)} \end{bmatrix} \cdot \begin{bmatrix} B_1 \\ B_2 \end{bmatrix}, \quad (19)$$

where B_1 and B_2 are unknown scalars; the other two eigenvalues of $[\underline{Q}]$ describe waves that amplify as $z \rightarrow \infty$ and cannot therefore contribute to the Dyakonov–Tamm wave. At the same time,

$$[\underline{f}(0-)] = \begin{bmatrix} 0 & \frac{\alpha_s}{k_o} \\ 1 & 0 \\ \frac{\alpha_s}{k_o} \eta_o^{-1} & 0 \\ 0 & -n_s^2 \eta_o^{-1} \end{bmatrix} \cdot \begin{bmatrix} A_s \\ A_p \end{bmatrix}, \quad (20)$$

by virtue of (9) and (10). Continuity of the tangential components of the electric and magnetic field phasors across the plane $z = 0$ requires that

$$[\underline{f}(0-)] = [\underline{f}(0+)], \quad (21)$$

which may be rearranged as

$$[\underline{M}] \cdot \begin{bmatrix} A_s \\ A_p \\ B_1 \\ B_2 \end{bmatrix} = \begin{bmatrix} 0 \\ 0 \\ 0 \\ 0 \end{bmatrix}. \quad (22)$$

For a nontrivial solution, the 4×4 matrix $[\underline{M}]$ must be singular, so that

$$\det [\underline{M}] = 0 \quad (23)$$

is the dispersion equation for the Dyakonov–Tamm wave. The value of κ satisfying (23) was obtained by employing the Newton–Raphson method [28].

3. Numerical Results and Discussion

We set $\lambda_o = 633$ nm in accordance with (6), since calculations were performed only for CTFs or SNTFs composed of titanium oxide. All calculations for the periodically nonhomogeneous SNTFs were performed for $\tilde{\chi}_v = 19.1^\circ$ and $\Omega = 197$ nm with two oscillation amplitudes: $\delta_v = 7.2^\circ$ and 16.2° . For comparison, calculations were

performed on CTFs for $\chi_v(z) \equiv 7.2^\circ$ and $19.1^\circ \forall z \geq 0$. The former is the approximate lower limit of χ_v obtainable with current STF technology. For a chosen set of values of n_s , $\tilde{\chi}_v$, and δ_v , surface-wave propagation was found to occur in four separate γ -ranges: $\gamma \in [\pm\gamma_m - \Delta\gamma/2, \pm\gamma_m + \Delta\gamma/2]$ and $\gamma \in [\pm\gamma_m + 180^\circ - \Delta\gamma/2, \pm\gamma_m + 180^\circ + \Delta\gamma/2]$. Here the angle $\gamma_m \in (0^\circ, 90^\circ)$ is used to describe the mid-point of a γ -range while $\Delta\gamma \leq 90^\circ$ is the extent of that range. Since the surface-wave characteristics are the same in all four γ -ranges, results are displayed only for $\gamma \in [\gamma_m - \Delta\gamma/2, \gamma_m + \Delta\gamma/2]$.

The magnitude of the phase velocity of the Dyakonov–Tamm wave was compared with that of the phase velocity of the bulk wave in the isotropic partnering material. For this purpose, we defined the relative phase speed

$$\bar{v} = v_{DT} n_s \sqrt{\epsilon_o \mu_o}, \quad (24)$$

where $v_{DT} = \omega/\kappa$ is the phase speed of the Dyakonov–Tamm wave.

Let us begin the presentation and discussion of results with the characteristics of Dyakonov waves guided by the interface of a CTF ($\delta_v = 0^\circ$) and an isotropic dielectric material [5]. Figure 3 shows plots of \bar{v} versus γ with: $\chi_v = 7.2^\circ$ for $n_s = 1.57, 1.59, 1.61, 1.63, 1.65, 1.67, 1.69, 1.71, \text{ and } 1.73$; and $\chi_v = 19.1^\circ$ for $n_s = 1.80, 1.82, \text{ and } 1.84$. Three characteristics of Dyakonov waves can be garnered from this figure:

- (i) the nearly vertical curves demonstrate the extremely small width $\Delta\gamma$ of the γ -range, leading to very narrow angular existence domains as we remarked upon in Section 1;
- (ii) higher values of n_s result in higher values of γ_m ; and
- (iii) lower values of χ_v also result in higher values of γ_m .

Figure 4 shows \bar{v} as a function of γ when $\tilde{\chi}_v = 19.1^\circ$ for three groups of parameters:

- $\delta_v = 0^\circ$ for $n_s = 1.80, 1.82, \text{ and } 1.84$;
- $\delta_v = 7.2^\circ$ for $n_s = 1.73, 1.77, 1.82, 1.88, 1.92, \text{ and } 1.96$; and
- $\delta_v = 16.2^\circ$ for $n_s = 1.80 \text{ and } 1.84$.

The first group has a CTF as the anisotropic partnering material, whereas the second and the third groups have a periodically nonhomogeneous SNTF serving that role. Immediately apparent is the *dramatic increase* in $\Delta\gamma$ brought about by the introduction of sinusoidal oscillation in the vapor incidence angle. With $\Delta\gamma$ on the order of tens of degrees when an SNTF is the anisotropic partnering material, the width of the γ -range is orders of magnitude greater than that obtained with a CTF as the anisotropic partnering material. As n_s increases, the γ -range supporting surface-wave propagation widens and the mid-point γ_m shifts to higher values. When $\delta_v = 16.2^\circ$ and n_s is increased to 1.84, $\Delta\gamma$ actually increases to 90° , which means that the four separate γ -ranges merge into one, thereby allowing surface-wave propagation to occur for any value of γ .

Figure 4 also indicates that the average value of \bar{v} over the γ -range rises as n_s increases, for both $\delta_v = 7.2^\circ$ and 16.2° . For a given value of γ , \bar{v} takes on similar values for CTFs and SNTFs.

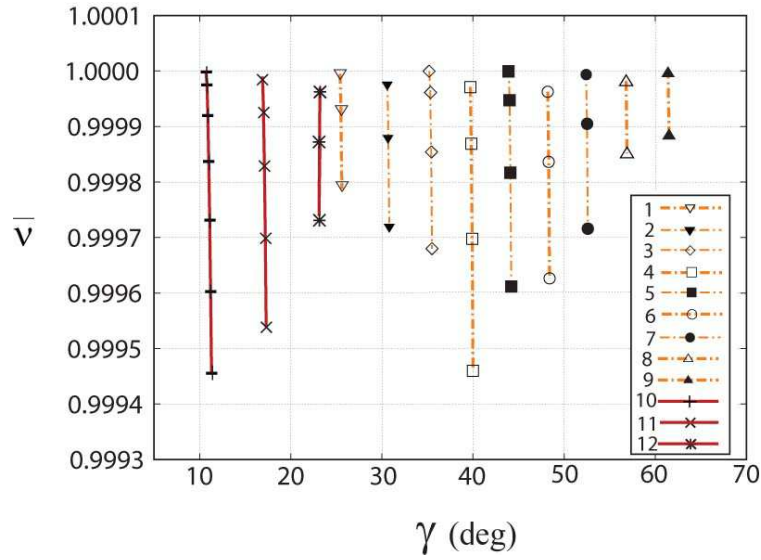


Figure 3. Relative phase speed \bar{v} as a function of γ when $\delta_v = 0^\circ$. The values of $\tilde{\chi}_v$ are as follows: (1)-(9) 7.2° , (10)-(12) 19.1° . The values of n_s are as follows: (1) 1.57, (2) 1.59, (3) 1.61, (4) 1.63, (5) 1.65, (6) 1.67, (7) 1.69, (8) 1.71, (9) 1.73, (10) 1.80, (11) 1.82, (12) 1.84.

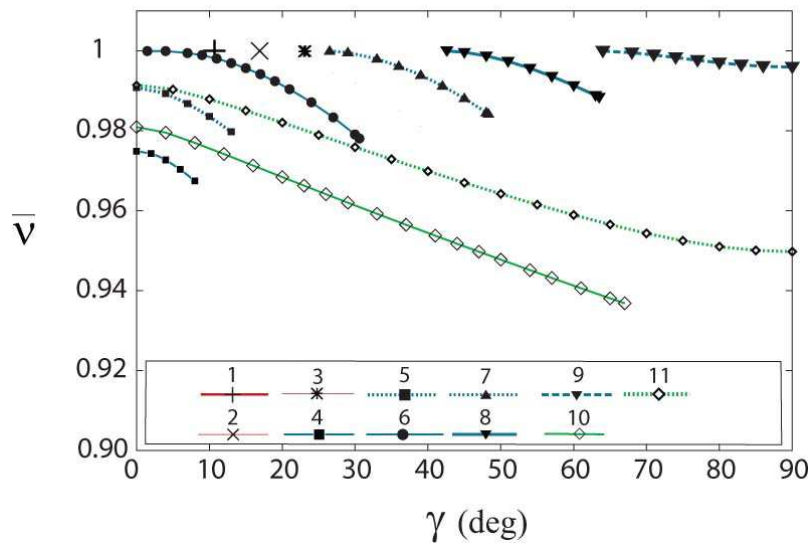


Figure 4. Relative phase speed \bar{v} as a function of γ when $\tilde{\chi}_v = 19.1^\circ$. The values of δ_v are as follows: (1)-(3) 0° , (4)-(9) 7.2° , (10) and (11) 16.2° . The values of n_s are as follows: (1) 1.80, (2) 1.82, (3) 1.84, (4) 1.73, (5) 1.77, (6) 1.82 (7) 1.88, (8) 1.92, (9) 1.96, (10) 1.80, (11) 1.84.

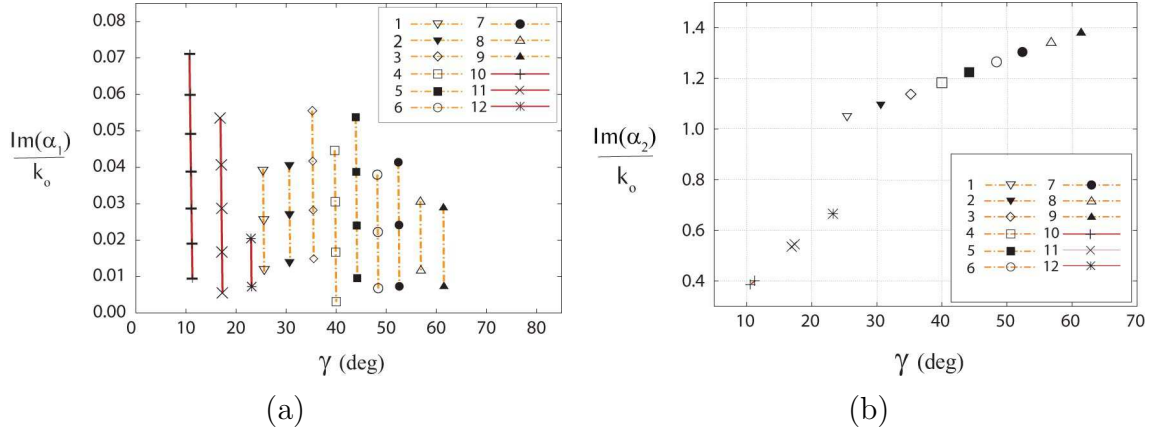


Figure 5. Normalized decay constants $\text{Im}[\alpha_1]/k_o$ and $\text{Im}[\alpha_2]/k_o$ as functions of γ when $\delta_v = 0^\circ$. The values of $\tilde{\chi}_v$ are as follows: (1)–(9) 7.2° , (10)–(12) 19.1° . The values of n_s are as follows: (1) 1.57, (2) 1.59, (3) 1.61, (4) 1.63, (5) 1.65, (6) 1.67, (7) 1.69, (8) 1.71, (9) 1.73, (10) 1.80, (11) 1.82, (12) 1.84.

The localization of the surface wave about the bimaterial interface is described by the decay constants $\text{Im}[\alpha_1]$ and $\text{Im}[\alpha_2]$ in the anisotropic partnering material and by $\text{Im}[\alpha_s]$ in the isotropic partnering material. Figure 5 displays the two decay constants in the CTF normalized to the free-space wavenumber, $\text{Im}[\alpha_1]/k_o$ and $\text{Im}[\alpha_2]/k_o$, as functions of γ for $\chi_v = 7.2^\circ$ and 19.1° for the same values of n_s as in Figure 3. The values of $\text{Im}[\alpha_1]/k_o$ show considerable variation over the γ -range for a given set of χ_v and n_s even though the γ -range is very narrow, as shown by the nearly vertical curves in Figure 5a. Unlike $\text{Im}[\alpha_1]/k_o$, $\text{Im}[\alpha_2]/k_o$ shows little variation over the γ -range and, for most values of n_s , appears as a single point in Figure 5b. Furthermore, $\text{Im}[\alpha_2]/k_o$ is roughly a linear function of γ with a positive slope, for a given value of χ_v . The slope increases as χ_v increases.

Figures 6 and 7) show the decay constants in the anisotropic partnering material as functions of γ for $\tilde{\chi}_v = 19.1^\circ$, the remaining parameters being the same as in Figure 4. The values of $\text{Im}[\alpha_1]/k_o$ in Figure 6a are larger in the SNTFs than they are in the CTFs for the same values of n_s and γ . The values of $\text{Im}[\alpha_1]/k_o$ appear to decrease towards zero at the upper range of γ for each value of n_s , except for those cases where the range of γ extends to 90° . In the two cases where the γ -range extends to 90° , $\text{Im}[\alpha_1]/k_o$ shows a minimum at 90° . It should be kept in mind that neither 0° nor 90° truly represent the limits of a γ -range for surface-wave propagation, since curves which seem to end at these points are joined to curves of one of the other three, in general, separate γ -ranges, thereby resulting in only two distinct γ -ranges.

Values of $\text{Im}[\alpha_2]/k_o$ in the SNTF when $\delta_v = 7.2^\circ$ are nearly identical to those in the CTF at a given value of γ , as shown in Figure 6b, for $\tilde{\chi}_v = 19.1^\circ$. The curves of $\text{Im}[\alpha_2]/k_o$ versus γ for the various values of n_s nearly join to form a single smooth continuous curve, except near $\gamma = 0^\circ$ where the curves for $n_s = 1.73$, 1.77 and 1.82 bifurcate. The value of $\text{Im}[\alpha_2]/k_o$ increases as n_s and γ increase.

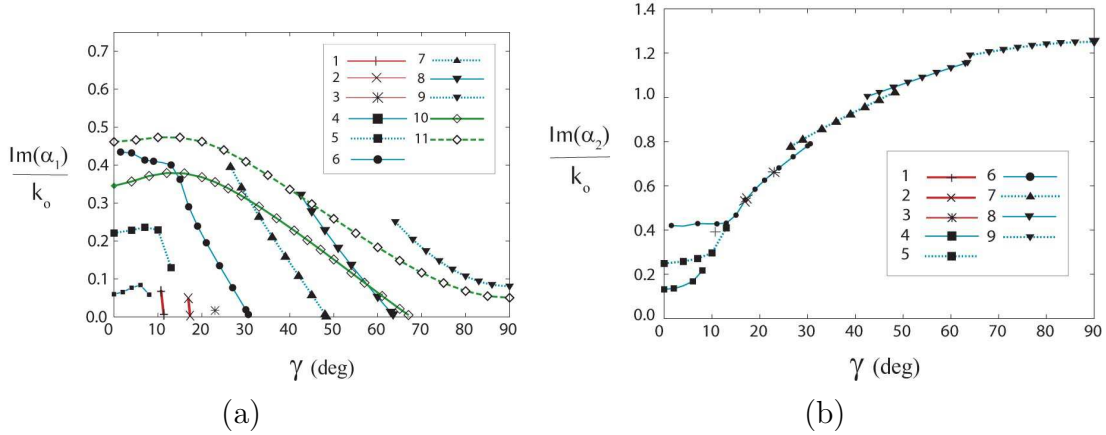


Figure 6. Normalized decay constants $\text{Im}[\alpha_1]/k_o$ and $\text{Im}[\alpha_2]/k_o$ as functions of γ when $\tilde{\chi}_v = 19.1^\circ$. The values of δ_v are as follows: (1)-(3) 0° , (5)-(9) 7.2° , (10) and (11) 16.2° . The values of n_s are as follows: (1) 1.80, (2) 1.82, (3) 1.84, (4) 1.73, (5) 1.77, (6) 1.82, (7) 1.88, (8) 1.92, (9) 1.96, (10) 1.80, (11) 1.84.

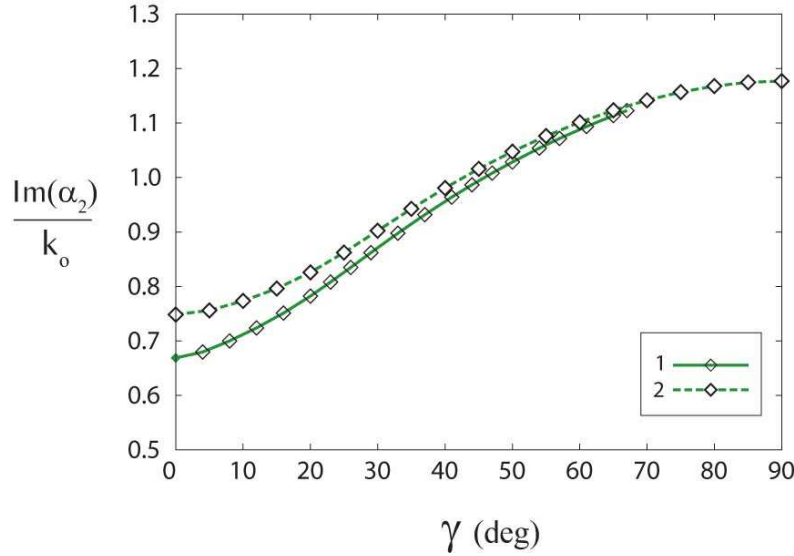


Figure 7. Normalized decay constant $\text{Im}(\alpha_2)/k_o$ as a function of γ when $\tilde{\chi}_v = 19.1^\circ$ and $\delta_v = 16.2^\circ$. The values of n_s are (1) 1.80, (2) 1.84.

The behaviour of $\text{Im}[\alpha_2]/k_o$ for higher modulation amplitude, $\delta_v = 16.2^\circ$, is presented in Figure 7 for $n_s = 1.80$ and 1.84. At low values of γ , $\text{Im}[\alpha_2]/k_o$ is larger for $\delta_v = 16.2^\circ$ than for $\delta_v = 7.2^\circ$. As γ approaches 90° , however, the value of $\text{Im}[\alpha_2]/k_o$ for $\delta_v = 16.2^\circ$, for both $n_s = 1.80$ and 1.84, approaches a value only slightly less that observed when $\delta_v = 7.2^\circ$ and $n_s = 1.96$.

The polarization state of the surface wave in the isotropic partnering material was also investigated. First, let us present data when the anisotropic partnering material is a CTF ($\delta_v = 0^\circ$). Figure 8 shows the ratio of the s -polarization amplitude to the the p -polarization amplitude for $n_s = 1.57, 1.59, 1.61, 1.63, 1.65, 1.67, 1.69, 1.71$, and

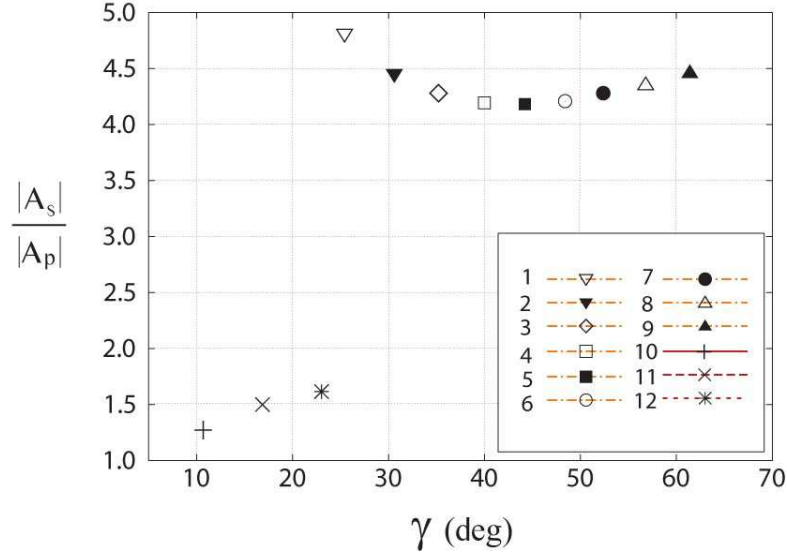


Figure 8. Ratio $|A_s|/|A_p|$ as a function of γ when $\delta_v = 0^\circ$. The values of $\tilde{\chi}_v$ are as follows: (1)-(9) 7.2° , (10)-(12) 19.1° . The values of n_s are as follows: (1) 1.57, (2) 1.59, (3) 1.61, (4) 1.63, (5) 1.65, (6) 1.67, (7) 1.69, (8) 1.71, (9) 1.73, (10) 1.80, (11) 1.82, (12) 1.84.

1.73 when $\tilde{\chi}_v = 7.2^\circ$; and for $n_s = 1.80, 1.82$ and 1.84 when $\tilde{\chi}_v = 19.1^\circ$. When the vapor incidence angle is low ($7.2^\circ \forall z \geq 0$), the surface wave in the isotropic partnering material is predominantly s -polarized with $4 < |A_s|/|A_p| < 5$. When the vapor incidence angle is increased to $19.1^\circ \forall z \geq 0$, the surface wave is only mildly polarized with $1 < |A_s|/|A_p| < 2$, and $|A_s|/|A_p|$ shows a positive slope as a function of γ .

Figure 9 shows the ratio $|A_s|/|A_p|$ versus γ , when $\tilde{\chi}_v = 19.1^\circ$, for CTFs ($n_s = 1.80, 1.82, 1.84$) and SNTFs with $\delta_v = 7.2^\circ$ ($n_s = 1.73, 1.77, 1.82, 1.88, 1.92, 1.96$). At the same values of γ , the values of $|A_s|/|A_p|$ are slightly smaller for the SNTF than the CTF. As with the curves describing $\text{Im}[\alpha_2]/k_o$ in Figure 6b, the curves describing $|A_s|/|A_p|$ for the SNTFs nearly join to form a single, continuous curve. At $\gamma = 0^\circ$, the surface wave is entirely p -polarized in the isotropic partnering material. The s -polarization state intensifies rapidly but then levels off at larger values of γ . The value of $|A_s|/|A_p|$ is nearly constant at ~ 1.6 for $\gamma > 60^\circ$. For $\delta_v = 19.1^\circ$, the behaviour of $|A_s|/|A_p|$ is similar, as shown in Figure 10, but plateaus at a value of about 1.3 at large values of γ .

4. Concluding Remarks

To conclude, we examined the phenomenon of surface-wave propagation at the planar interface of an isotropic dielectric material and a sculptured nematic thin film with periodic nonhomogeneity. The boundary-value problem was formulated by marrying the usual formalism for the Dyakonov wave at the planar interface of an isotropic dielectric material and a columnar thin film with the methodology for Tamm states in solid-state physics. The solution of the boundary-value problem led us to predict the existence of

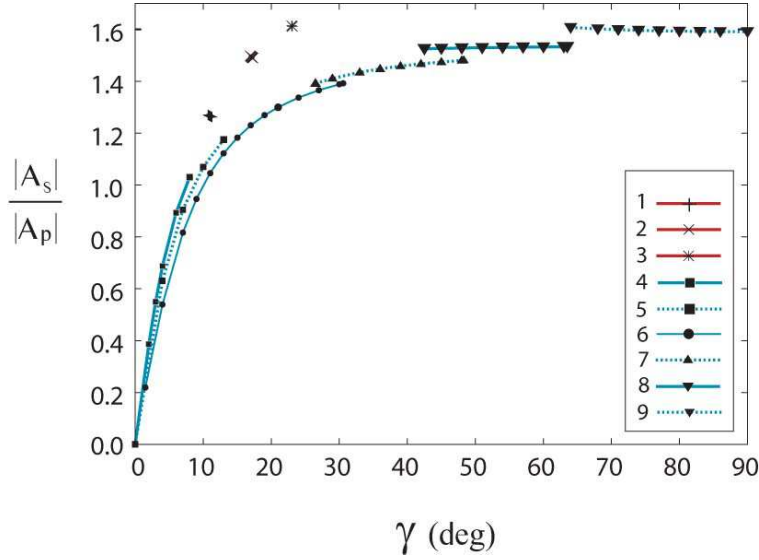


Figure 9. Ratio $|A_s|/|A_p|$ as a function of γ when $\tilde{\chi}_v = 19.1^\circ$. The values of δ_v are as follows: (1)-(3) 0° , (4)-(9) 7.2° . The values of n_s are as follows: (1) 1.80, (2) 1.82, (3) 1.84, (4) 1.73, (5) 1.77, (6) 1.82, (7) 1.88, (8) 1.92, (9) 1.96.

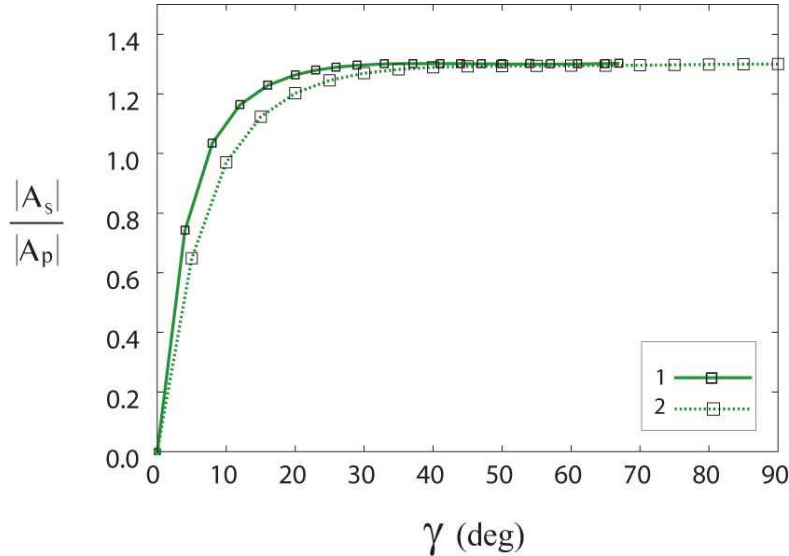


Figure 10. Ratio $|A_s|/|A_p|$ as a function of γ when $\tilde{\chi}_v = 19.1^\circ$ and $\delta_v = 16.2^\circ$. The values of n_s are (1) 1.80 and (2) 1.84.

Dyakonov–Tamm waves.

Dyakonov surface waves *may* propagate guided by the bimaterial interface of an isotropic dielectric material and a columnar thin film (or any other biaxial dielectric material). The angular domain of their existence is very narrow, of the order of a degree. Although several techniques have been suggested [2, 7], the widening of that domain has not been impressive. By periodically distorting the CTF in two ways, either as a chiral STF [8] or now as a periodically nonhomogeneous SNTF, the angular existence

domain for surface (Dyakonov–Tamm) waves can be widened dramatically, even to the maximum possible. A search for Dyakonov–Tamm waves is, at the present time, the most promising route to take for experimental verification of surface-wave propagation at the interface of two dielectric materials at least one of which is anisotropic.

In Section 1, we posed the following question: Is the huge angular existence domain of Dyakonov–Tamm waves for the case investigated by Lakhtakia and Polo [8] due to the periodicity or due to the structural chirality of the chiral STF? Although the two attributes are inseparable in a chiral STF, our results in Section 3 indicate that the periodic nonhomogeneity is the responsible attribute.

Acknowledgment. This work was supported in part by the Charles Godfrey Binder Endowment at Penn State. KA thanks the Department of Engineering Science and Mechanics, Penn State, and AL is grateful to the Department of Physics, IIT Kanpur, for hospitality.

References

- [1] D'yakonov M I 1988 *Sov. Phys. JETP* **67** 714
- [2] Takayama O, Crasovan L-C, Johansen S K, Mihalache D, Artigas D and Torner L I 2008 *Electromagnetics* **28**, 126
- [3] Crasovan L C, Artigas D, Mihalache D and Torner L I 2005 *Opt. Lett.* **30** 3075
- [4] Artigas D and Torner L I 2005 *Phys. Rev. Lett.* **94** 013901
- [5] Polo J A Jr, Nelatury S R and Lakhtakia A 2007 *J. Nanophoton.* **1** 013501
- [6] Abdulhalim I, Zourob M and Lakhtakia A 2007 In: Marks R, Cullen D, Karube I, Lowe C R and Weetall H H (eds) *Handbook of Biosensors and Biochips* (Chicester, United Kingdom: Wiley) pp. 413–446
- [7] Nelatury S R, Polo J A Jr and Lakhtakia A 2008 *Microw. Opt. Technol. Lett.* **50** 2360
- [8] Lakhtakia A and Polo J A Jr 2007 *J. Eur. Opt. Soc.—Rapid Pub.* **2** 07021
- [9] Lakhtakia A and Messier R 2005 *Sculptured Thin Films: Nanoengineered Morphology and Optics* (Bellingham, WA, USA: SPIE Press).
- [10] Tamm I 1932 *Phys. Z. Sowjetunion* **1** 733
- [11] Ohno H, Mendez E E, Brum J A, Hong J M, Agulló-Rueda F, Chang L L and Esaki L 1990 *Phys. Rev. Lett.* **64** 2555
- [12] Lakhtakia A (ed) 1990 *Selected Papers on Natural Optical Activity* (Bellingham, WA, USA: SPIE)
- [13] Charney E 1985 *The Molecular Basis of Optical Activity* (Malabar, FL, USA: Krieger)
- [14] van de Hulst H C 1981 *Ligh Scattering by Small Particles* (New York, NY, USA: Dover) Sec. 6.4.
- [15] Mackay T G 2008 *J. Nanophoton.* **2** 029503
- [16] Bose J C 1898 *Proc. R. Soc. Lond. A* **63** 146
- [17] Ro R 1991 Determination of the electromagnetic properties of chiral composites, using normal incidence measurements, Ph.D. dissertation, Pennsylvania State University, University Park, PA, USA
- [18] Lakhtakia A 1994 *Beltrami Fields in Chiral Media* (Singapore: World Scientific)
- [19] Gómez Á, Lakhtakia A, Margineda J, Molina-Cuberos G J, Núñez J, Ipiña J S, Vegas A and Solano M A 2008 *IEEE Trans. Microw. Theory Tech.* **56** 2815
- [20] Whites K W and Chung C Y 1997 *J. Electromagn. Waves Applics.* **11** 371
- [21] Chandrasekhar S 1992 *Liquid Crystals* (Cambridge: Cambridge University Press)
- [22] Hodgkinson I J and Wu Q-h 1997 *Birefringent Thin Films and Polarizing Elements* (Singapore:

World Scientific)

- [23] Mattox D M 2003 *The Foundations of Vacuum Coating Technology* (Norwich, NY, USA: Noyes Publications)
- [24] Hodgkinson I J, Wu Q H and Hazel J 1998 *Appl. Opt.* **37** 2653
- [25] Chen H C 1992 *Theory of Electromagnetic Waves* (Fairfax, VA, USA: TechBooks).
- [26] Motyka M A and Lakhtakia A 2008 *J. Nanophoton.* **2** 021910
- [27] Yakubovich V A and Starzhinskii V M 1975 *Linear Differential Equations with Periodic Coefficients* (New York, NY, USA: Wiley).
- [28] Jaluria Y 1996 *Computer Methods for Engineering* (New York, NY, USA: Brunner–Routledge)